Microgravity Sci. Technol. (2017) 29:81–89
DOI 10.1007/s12217-016-9527-4

ORIGINAL ARTICLE

Ring-Sheared Drop (RSD): Microgravity Module for Containerless Flow Studies

Shreyash Gulati[1] · Aditya Raghunandan[1] · Fayaz Rasheed[1] · Samantha A. McBride[1] · Amir H. Hirsa[1]

Received: 24 July 2016 / Accepted: 4 November 2016 / Published online: 21 November 2016

Abstract Microgravity is potentially a powerful tool for investigating processes that are sensitive to the presence of solid walls, since fluid containment can be achieved by surface tension. One such process is the transformation of protein in solution into amyloid fibrils; these are protein aggregates associated with neurodegenerative diseases such as Alzheimer's and Parkinson's. In addition to solid walls, experiments with gravity are also subject to influences from sedimentation of aggregates and buoyancy-driven convection. The ring-sheared drop (RSD) module is a flow apparatus currently under development to study formation of amyloid fibrils aboard the International Space Station (ISS). A 25 mm diameter drop of protein solution will be contained by surface tension and constrained by a pair of sharp-edged tubes, forming two contact rings. Shear can be imparted by rotating one ring with the other ring kept stationary. Here we report on parabolic flights conducted to test the growth and pinning of 10 mm diameter drops of water in under 10 s of microgravity. Finite element method (FEM) based fluid dynamics computations using a commercial package (COMSOL) assisted in the design of the parabolic flight experiments. Prior to the parabolic flights, the code was validated against experiments in the lab (1 g), on the growth of sessile and pendant droplets. The simulations show good agreement with the experiments. This modeling capability will enable the development of the RSD at the 25 mm scale for the ISS.

✉ Amir H. Hirsa
hirsaa@rpi.edu

[1] Rensselaer Polytechnic Institute, Troy, New York, NY, USA

Keywords Fluid dynamics · Proteins · Parabolic flight · Drop growth · Drop pinning · Contact angle

Introduction

Fluid dynamics and biophysics are among the fields that can benefit significantly from microgravity. Microgravity allows for elimination of effects such as buoyancy-driven convection and sedimentation which complicate experiments on Earth. Elimination of gravity also permits surface tension to provide fluid containment and is especially beneficial for conducting experiments that are negatively influenced by the presence of container walls. Complications associated with solid walls that can influence liquid solutions include chemical, sorption, and electrostatic interactions. In order to conduct these experiments in microgravity, reliable procedures for growing and constraining the drops must be established.

A variety of microgravity experiments involving growth and manipulation of liquid drops have been performed in the past to study physical phenomena including contact angle dynamics and wetting, drop coalescence, evaporation, combustion and stability of emulsions. Nayagam et al. (1998) investigated combustion of n-heptane drops in microgravity using the multi-user droplet combustion apparatus (MDCA). In these experiments, they used a pair of opposed syringe needles to deploy n-heptane drops of 1.5 to 5 mm diameter. L-shaped hypodermic needles with their motion controlled by servo motors came in tangentially from opposite directions to create the drop. This was followed by withdrawal of the needles at a high acceleration and subsequent ignition of the drop using hot-wire igniters. Antar et al. (2003) performed drop coalescence experiments

to measure the viscosity of highly viscous undercooled liquids. They grew two drops of 8 to 15 mm diameter using two hypodermic needles which were contacted using manual force, allowing the drops to coalesce. Savino et al. (2003) examined wetting and coalescence of silicone oil sessile drops formed over copper substrates in Flourinert (a coolant liquid). They grew sessile drops of 10 mm contact diameter using a cylindrical copper needle with a coaxial hole. Marangoni flow was induced in the drop by heating the needle via a heating element coiled around it. The drop was then contacted against a cooled copper substrate. Chiang and Elliott (2005) developed an emulsion droplet system to study the effects of solid particles on the stability of emulsions. In their experiment, glass-bead-coated water drops of up to 12 mm diameter were created in an oil-filled container and made to coalesce. Effects of gravity on contact angle and drop interface behavior was studied by Brutin et al. (2009). They created sessile drops on the flat end of a cylindrical substrate with liquid flowing through the hole along the axis of the substrate. The contact diameter of sessile drops created by Brutin et al. (2009) was in the range of 4 to 10 mm. Brutin et al. (2010) used a similar experimental setup to investigate evaporation of ethanol sessile drops over a heated polytetrafluoroethylene (PTFE) substrate. Although growth of drops in microgravity have been reported, a constrained drop where flow can be driven by interfacial viscosity has not been presented.

Of the many studies that can benefit from containerless experimentation, ring-sheared drop (RSD) module is currently focused on the formation of amyloid fibrils. Fibril plaque accumulation in the brain is associated with numerous neurodegenerative diseases, including Alzheimer's and Parkinson's. It is known that shearing flows as well as interfacial effects can vastly alter fibril structure and formation kinetics (Bekard et al. 2011; McBride et al. 2015). This is significant because shearing occurs in the presence of fluid interfaces for a variety of bioprocesses (Bekard et al. 2011). In studies where air-water interfaces were prominent (Sluzky et al. 1991; Maa and Hsu 1997; Nielsen et al. 2001; Morinaga et al. 2010), fibrillization was accelerated. Results from our laboratory have demonstrated that fluid interfaces are especially effective at inducing amyloid fibrils when they are sheared (Posada 2013), but the influence of container walls is not clear. The ring-sheared drop module utilizes the microgravity environment in which amyloidogenesis studies can be performed with large-scale liquid systems without a container, since surface tension provides containment of the liquid.

Development of the ring-sheared drop module was motivated by the desire to perform shearing flow experiments on protein solution in the absence of solid walls to study the formation of amyloid fibrils. In the RSD module, presented in Fig. 1, a pair of sharp-edged tubes constrain a drop of protein solution along two contact regions or rings. Note, RSD for implementation aboard the ISS has a diameter ($2R_d$) of 25 mm, and the contact rings have a diameter ($2R_r$) of 15 mm. This geometric configuration forms a 3-4-5 triangle between the pinned corner of the drop, the center of the rings and the center of the drop, as depicted in Fig. 1. The large syringe needle used for growing the drop has an outer diameter ($2R_o$) of 3.4 mm. One of the rings is stationary and the other can rotate at specified rates. Rotation of one ring shears the interface which in-turn drives flow in the bulk through the action of surface shear viscosity. The effectiveness of surface shear viscosity in driving a flow throughout the drop was demonstrated with a knife-edge viscometer, both computationally and experimentally (Raghunandan et al. 2015).

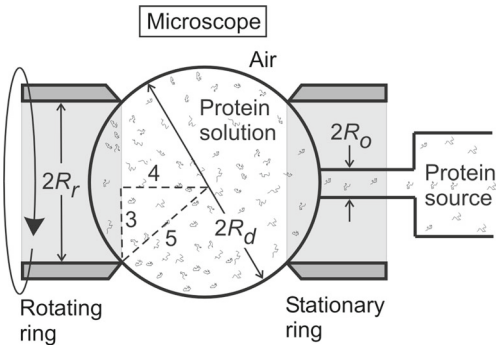

Fig. 1 Ring-sheared drop module. The schematic shows a drop of protein solution constrained by two sharp-edged tubes forming two contact rings. One contact ring is stationary and the other can rotate at specified rates. A syringe needle connected to the source of protein solution is used to grow the drop

Aside from studying amyloid fibril formation, the RSD module can also be utilized in the future as a containerless bioreactor for performing interfacial studies with microorganisms. Furthermore, increased utilization of interfacial processing in the pharmaceutical industry (Hayes 2011) may benefit from the RSD for other biomolecular studies, since this module provides unique capabilities in interfacial bioprocessing.

Besides drop growth and pinning, stability of the drop also impacts the geometric configuration of the RSD which plays a crucial role in its operation. Bostwick and Steen (2015) review the stability of spherical drops constrained in various ways.

For the successful development and implementation of the RSD, the physical phenomena of drop growth, pinning, and stability must be studied in detail. The size of drops that can be created on the ground is limited by gravity to about the capillary length, namely ~2 mm for water in air. Hence, parabolic flight experiments were conducted to test the growth and pinning of larger (10 mm diameter) drops of water within 10 s of microgravity. Finite element

method (FEM) based fluid dynamics computations were performed to predict the behavior of the drop while it grew and pinned to the rings. A preliminary computation considering only the drop deployment phase (and not including the pinning by the rings) was performed to double check that the flow rate used was not too high to make the shape of the growing drop noticeably non-spherical. Spherical shape of the drop simplified the experiment by simultaneous contacting of the drop to the far-side ring at the end of the growth process. The slow rate of the drop growth process also ensured that there were no hydrodynamic instabilities. Hence, the computations assisted the design of the setup for the parabolic flight experiment. Further, the computational models were validated against corresponding measurements on pendant and sessile drop (1 g) experiments (prior to the parabolic flight) and microgravity experiments (post the parabolic flight). These validated computational models can be used to assist the design of future parabolic flight experiments that are planned to test growth and pinning of larger drops. Ultimately, these validated computational models will be utilized to aid the design of the hardware for the implementation of RSD aboard the ISS.

Experimental Setup and Procedures

Ground-Based (1 g) Experiments

The setup for ground-based experiments is shown in Fig. 2a. Water droplets were grown at the tip of a 10 gauge stainless steel syringe needle (Hamilton, 91010) with an outer diameter (OD) of 3.4 mm and an inner diameter (ID) of 2.7 mm connected to a 2.5 mL gas-tight glass syringe (Hamilton, 81420) via PTFE tubing. The needle was press fitted into an acrylic block which was secured onto an optics table. The needle was mounted pointing downward to grow pendant drops and pointing upward to create sessile droplets. The rate of droplet growth was controlled by a syringe pump (KD Scientific, Legato 210) and a fixed flow rate of 0.087 mL/s corresponding to deployment of a 10 mm diameter drop in 6 s during the parabolic flight experiment, was chosen for all the ground-based experiments. The experiments were performed using de-ionized (DI) water of resistivity greater than 18.2 MΩ cm and total organic carbon content less than 5 ppb (Millipore, Simplicity 185-UV, fed with Type-1 DI water).

A fiber optic light source (Dolan-Jenner, MI-150) was used to backlit the droplets. The droplet growth and subsequent pinch-off was captured using a DSLR camera (Nikon, D5300) and a microscope (Optem, Zoom 70XL lens with a 1.5X objective). Since hemishperical interfaces can be modeled quite conveniently in the computations, prior to start of each experiment a hemispherical cap of water with diameter equal to the OD of the needle was created using a flow rate of 0.001 mL/s. This was followed by a waiting time of a few minutes to allow the hemispherical drop reach a quiescent state.

Parabolic Flight Experiments

Experiments were performed during parabolic flights offered by a commercial provider (Zero Gravity Corp., Boeing 727) over a total of 50 parabolas. Each cycle comprised ~40 s of hypergravity (>1 g) followed by ~20 s of microgravity (<0.05 g). Figure 2b shows the hardware for the parabolic flight experiments. The setup was designed to grow and pin 10 mm diameter water drops between two sharp-edged glass tubes (in a similar way as shown in Fig. 1,

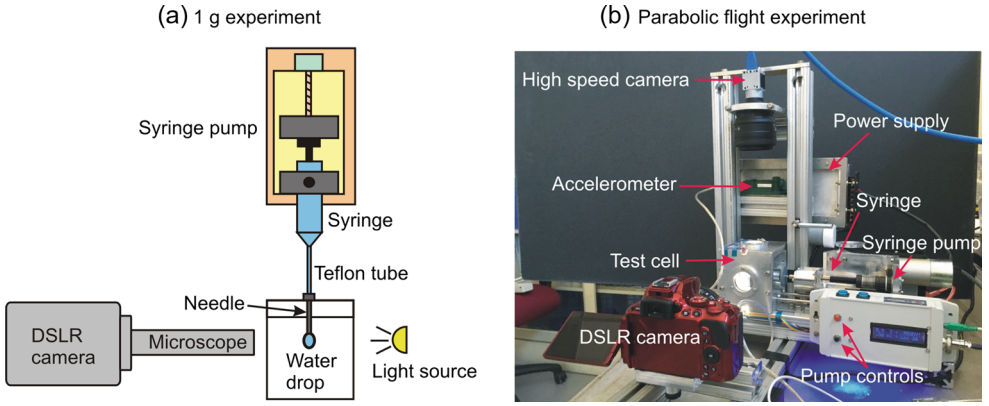

Fig. 2 **a** Schematic of the setup for ground-based (1 g) experiments that includes a syringe pump, a syringe, a PTFE tube and a syringe needle to create millimeter scale water droplets. A digital single-lens reflex (DSLR) camera viewed the backlit drop. **b** Photograph of the setup for parabolic flight experiments, which includes a test cell where a centimeter scale water drop was grown and pinned between two sharp-edged glass rings using a syringe and needle operated by a syringe pump. A DSLR camera viewed the drop from front while a high-speed camera was used to observe the drop from top. An accelerometer was mounted on the frame of the setup (courtesy of NASA MSFC)

but with both rings non-rotating), in 6 s of microgravity. The glass tubes were cut to a length of 38 mm from a stock of precision glass tube with an ID of 6.1 mm (Ace Glass, 8700 Trubore). One end of each tube was ground flat and polished using 400 grit sandpaper to ensure orthogonality with respect to the axis of the tube. To achieve this, the glass tube was epoxied to the shank of a drill bit and the assembly was slowly rotated in a vertical mill while being lowered manually to make contact with the sandpaper bonded to a machinist block. Subsequently, this squared end was beveled on the outside as depicted in Fig. 1, using a high-speed die grinder mounted at 45° on the vertical mill table. Following the beveling process, the unmachined end of the glass tube was press fit into nylon bushings which could thread into two opposing vertical faces of an aluminum test cell. The distance between the beveled glass tubes which pin the drop could be adjusted by rotating the nylon bushings and was set to 8 mm for the microgravity experiments, achieving a 3-4-5 triangle with rings of 6 mm nominal ID, held 8 mm apart, constraining a 10 mm diameter drop. It should be noted that, the beveled ends were dip-coated with a hydrophobic coating (Scotchgard) to prevent the drop from wetting the beveled end of the glass tubes.

An OEM-type syringe pump (Hamilton, PSD3) was used to grow the drop from the tip of a stainless steel needle (10 gauge, same as that used in the ground-based experiments) fitted on a 5 mL gas-tight glass syringe (Hamilton, Model 1005). The pump was controlled by an Arduino-based, custom made system. The syringe was pre-filled with 3.1 mL of DI water (sufficient for 5 deployments). The drop volume and deployment time were set to 0.52 mL (corresponding to a 10 mm drop) and 6 s, respectively. The syringe pump was mounted on a metal block that could slide on a rail to facilitate the axial movement of the needle inside the glass tube. For drop deployment, the needle was moved back to a distance of 1 mm behind the edge of one of the tube (ring location).

The test cell was equipped with two circular glass windows to view the drop from front and top. Four LED lights were attached to the corners of the test cell at 45°, 135°, 225°, and 315°. A DSLR camera (Nikon, D5500), fitted with a macro zoom lens (Nikkor, AF-S DX 18-55mm f/3.5-5.6G VR II) and a high-speed camera (Basler, ace acA2000-165uc Color USB 3.0), fitted with a primary lens (Nikkor, AF-S DX 35 mm f/1.86G) were used to view the drop from the front and the top. All components (test cell, syringe pump, cameras, etc.) were fixed on an L-shaped structural frame with a side arm. To record the g-level experienced by the equipment, an accelerometer (Extech, VB300) was mounted on the frame between the high-speed camera and the test cell. The temperature and pressure variations during the experiments were recorded using an independent sensor (Pyle, PTHDL170). The entire setup was secured to the floor of the aircraft by clamping the frame to a base plate that was bolted to the floor. To prevent aircraft vibrations from affecting the experiment, nylon tethers were attached to the structural frame. This allowed the setup to float freely (thus isolated from aircraft vibrations) during the microgravity, if deemed necessary, while still remaining secured to the base plate.

A typical experiment of drop deployment and pinning was performed during one cycle of microgravity which lasted for ∼20 s. For each experiment, pressing the trigger button on the control system advanced the needle through the glass tube to a fixed distance of 1 mm behind the edge of the ring on the side of the needle. The next trigger deployed the drop in 6 s. As the drop was being deployed, it would pin, first to the ring nearer to it, and, with continued growth, subsequently pinned to the opposite ring. At the end of the microgravity conditions, the drop would fall because of hypergravity. Any residual water in the glass tubes was simply soaked up using lens paper wrapped on popsicle sticks during the hypergravity part of the next parabola. Syringes with fresh liquid were replaced during the break between each set of 5 parabolas.

Experiments were performed over the course of two flight days. For the initial 5 parabolas on day-1 (Feb. 25, 2016), the setup was clamped to the floor of the aircraft. For the next 5 parabolas, the setup was freely floated by using the tethers securing it to the floor. The setup was clamped to the floor again for the last 5 parabolas. Video evidence from day-1 demonstrated that clamping the setup to the floor and thus subjected to aircraft vibrations, had negligible impact on the drop growth and pinning. Therefore, for simplicity of operation and added safety, the setup was clamped to the floor for all experiments on day-2 (Feb. 27, 2016). A total of 35 parabolas were performed on day-2.

Computational Modeling

FEM-based modeling using a commercial software package (COMSOL, with microfluidics module) was performed to simulate drop growth for the pendant (1 g), sessile (1 g) and parabolic flight tests. Additionally, pinning of the drop to the two contact rings was also modeled for the microgravity case. A schematic of the computational domain is presented in the Fig. 3. An axisymmetric model was constructed. Since air has a viscosity that is nearly two orders of magnitude smaller than that of water and a density that is about three orders of magnitude smaller than that of water, it does not impact the dynamics of drop growth. Hence, only the region containing water was included in the computational domain. For this computational model, Reynolds number is defined as $Re = 2wR_i/\nu$, where w is the axial

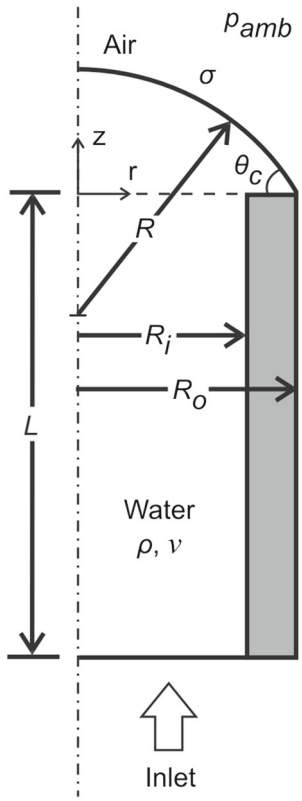

Fig. 3 Schematic of the computational domain. An axisymmetric model was used with mass flow boundary condition applied at the tube inlet and surface tension boundary condition applied at the air-water interface. The delivery tube walls were modeled as no-slip surfaces

velocity of the liquid averaged across the syringe needle, R_i is the inner radius of the syringe needle, and ν is the kinematic viscosity of the liquid. Reynolds number was found to be 48 and 37 respectively for the 1 g and microgravity cases. Since Re < 2100, the flow is laminar. For microgravity experiments, the syringe needle was modeled as a tube with length L equal to 50.8 mm. In the 1 g cases, the syringe needle and the PTFE tube were modeled as a combined tube with ID and OD equal to those for the needle since the tube diameter (2.4 mm) was close to the needle ID. The length of this equivalent tube was equal to 505 mm (same as combined length of the PTFE tube and the syringe needle).

A mass flow boundary condition, $\dot{m} = f\rho Q$ was applied at the tube inlet, where ρ is the density of the liquid, $Q = 0.087$ mL/s is the volume flow rate, and $f(t)$ is a dimensionless function that was used to represent the finite ramp up of the syringe pump. The default smoothed step function available in COMSOL ($f(t)$) was used to model the finite ramp up time ($t_0 = 0.066$ s) of the syringe pump used in the laboratory for the 1 g cases, while no such step function was used (i.e. $f(t) \equiv 1$) in the microgravity case because the syringe pump used in the microgravity setup had a negligible ramp up time. An "external fluid interface" boundary condition (surface tension boundary condition) was applied at the air-water interface with σ as the surface tension coefficient for pure water in air, and P_{amb} as the ambient air pressure. A gravitational pull was applied on the droplet by adding a body force for the 1 g cases. No-slip boundary condition was imposed on the delivery tube walls including the blunt end. The initial interface was hemispherical with the radius of curvature, $R = R_o$, where R_o is the outer radius of the needle and contact angle on the blunt end, $\theta_c = 90°$. The contact line of the water drop was fixed to the syringe needle at the outer radius. For the microgravity case, the numerical simulation was stopped when the diameter of the drop at the ring location (end of the glass tube) became equal to the ring diameter (glass tube ID) by using a "stop condition." This happens first when the drop contacts the ring on the same side as the needle and later when the drop contacts the other ring. After each contact event, new boundary conditions were introduced to fix the contact line at the ring and the simulation was continued. The Navier-Stokes equations were solved in the domain using COMSOL's laminar two-phase flow, moving mesh feature. This feature allowed the mesh inside the drop to deform while it grew, based on an arbitrary Lagrangian Euler (ALE) method. Winslow method was used for mesh smoothing. Automatic remeshing feature was also used with a "mesh quality cutoff" of 0.2 (default setting). The initial (time, t = 0) mesh contained 174,948 triangular mesh elements for the pendant (1 g) and sessile (1 g) cases. There were 20,244 triangular mesh elements in the domain for the microgravity case. A finer mesh with mesh element size of 0.045 mm was used for the protruding drop region while a coarser mesh with mesh element size of 0.1 mm was used for the tube region. A mesh refinement study was performed for all the cases which showed that further refinement of the mesh changed the results by less than 2 %. A time step (Δt) of 0.001 s was used. Courant number, $C = w\Delta t/\Delta x$, where Δx is the size of mesh elements in the domain, was found to be $C = 0.68$. Thus, the Courant–Friedrichs–Lewy condition, $C < 1$, was readily satisfied.

Results and Discussion

The shape of pendant and sessile droplets was measured in the lab (1 g) and compared to the COMSOL model prediction. The droplet shape predicted by computations, represented by green outlines, was overlaid with the corresponding snapshots from the experiments. Figure 4 shows the comparison between the computed and measured droplet shapes for the pendant and sessile drop (1 g) cases. Good agreement was observed from 0 to 0.4 s in the pendant (1 g) case. However, there was a departure between computation and measurement beyond 0.4 s due to the fact that in the

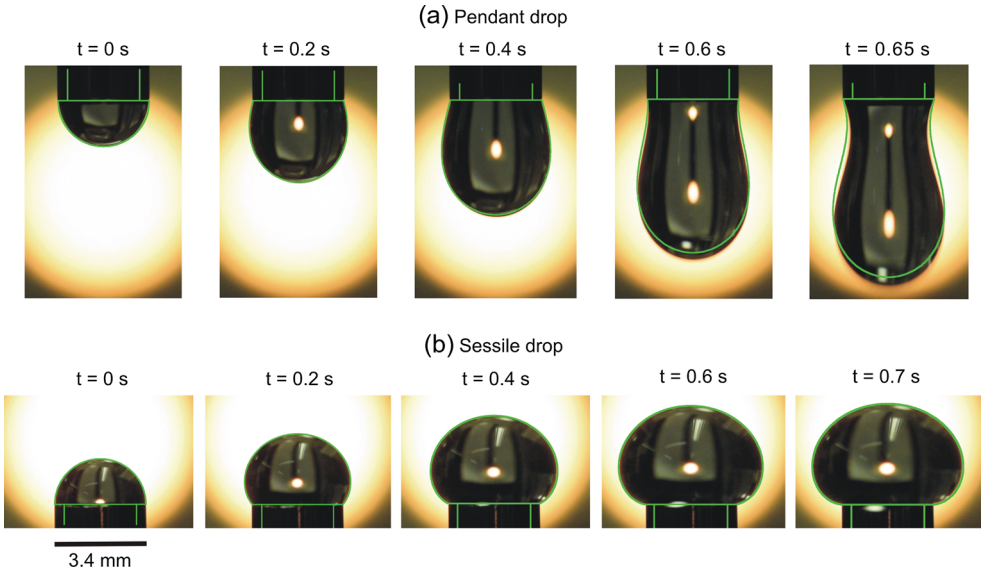

Fig. 4 Comparison of computed and measured droplet shapes for **a** pendant (1 g) case and **b** sessile (1 g) case. The *green outlines* represent the computed droplet shape

experiments, the drop pinned at about 97 % of the needle OD as shown in the Fig. 5a, whereas in the original numerical simulation the drop was pinned at the needle OD. This was confirmed by the results shown in the Fig. 5b which demonstrate that the computed droplet shape matched fairly with the measured droplet shape for all the time points on changing the pinning diameter to $0.97D_o$ in the numerical simulation. The droplet shape comparison was limited to 0.65 s beyond which pinch-off occurs. Pinch-off occurs very rapidly and is difficult to capture either experimentally or computationally (Chen et al. 2002).

In the sessile (1 g) case, the computation predicted droplet shape agrees with the experiment for all the time points. The droplet de-pins from the needle at around 0.7 s and therefore the drop shape comparison for the sessile (1 g) case was limited to that time point.

Figure 6 shows the comparison of the drop shapes from computations and experiments for the parabolic flight (microgravity) case. The figure shows that the computed drop shape agrees with the experiment up to 0.65 s. Due to a small radial misalignment of the syringe needle (∼0.5 mm or ∼15 % of the needle OD) inside the needle-side glass

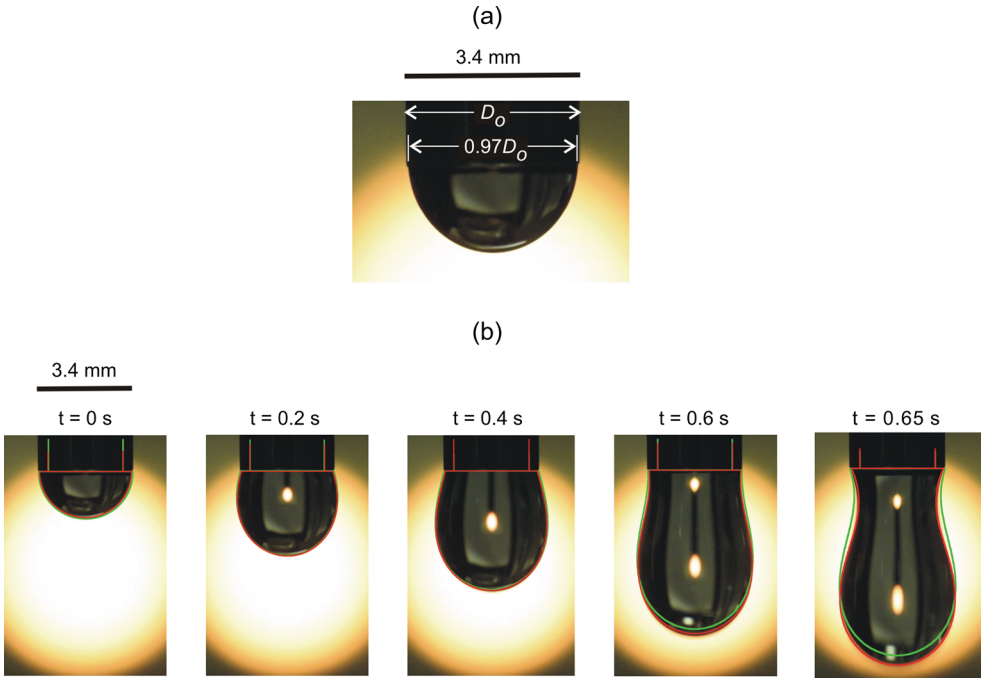

Fig. 5 **a** Picture of the drop showing pinning at 97 % of the needle OD **b** Comparison of computed and measured droplet shapes for pendant (1 g) case with the measured shape for pinning at D_o represented by the *green outlines* and that for pinning at $0.97D_o$ represented by the *red outlines*

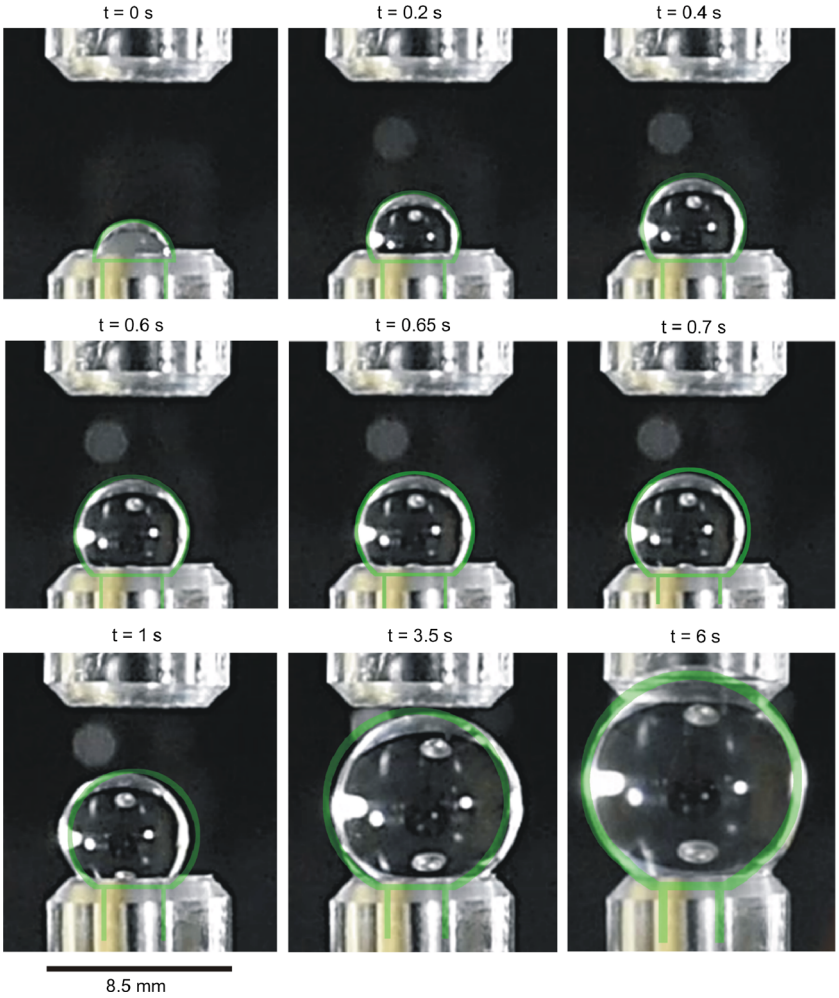

Fig. 6 Comparison of the computed and measured drop shapes for the microgravity case. The *green outlines* represent the computed drop shape

tube, the drop partially pinned to the left portion of the ring at around 0.7 s. Also, at the beginning of drop deployment, the needle was not located at the design location of 1 mm behind the end of the tube. Instead the needle was at around 0.4 mm behind the end of the tube or 0.6 mm (∼18 % of the needle OD) from its design location. Note, if the needle was concentric with the glass tube and at its design location, then the drop would have likely pinned the glass tube completely and symmetrically at a much later time; computations predict pinning at 2.9 s. The misalignment and improper location of the needle likely caused the disagreement between the computed and measured drop shape for t = 0.7 s to 3.5 s. At the end of the drop formation process, i.e. t = 6 s, a good agreement was observed between the computed and measured drop shape due to pinning of the drop on both rings that negated the impact of geometric imperfections and the resultant deviations observed earlier.

The contact angle, θ_c, was compared between the computations and experiments for the 1 g cases and the results are presented in Fig. 7a. Contact angle was measured using the DropSnake plugin in ImageJ (Stalder et al. 2006). It was observed that the contact angle from the computations agreed well with that from the 1 g experiments, see Fig. 7a. A similar comparison of computed and measured contact angles for the microgravity case was not possible because the resolution of the images taken from the microgravity experiments was not adequate to measure the contact angle accurately. Also, the maximum radius, R_{max}, and the maximum height, Z_{max}, were compared between the computations and the experiments, see Fig. 7b and c. The values of R_{max} and Z_{max} for the experiments were obtained by measuring the actual distances using ImageJ. A good agreement was observed between the computed and measured values of R_{max}. Computed Z_{max} agreed well with that measured from the experiments for all time points for the 1 g cases and up to 0.65 s for the microgravity case. Beyond 0.65 s, computed Z_{max} agreed only fairly with the measured value and not perfectly because of the early, partial pinning of the drop to the glass tube, as explained earlier.

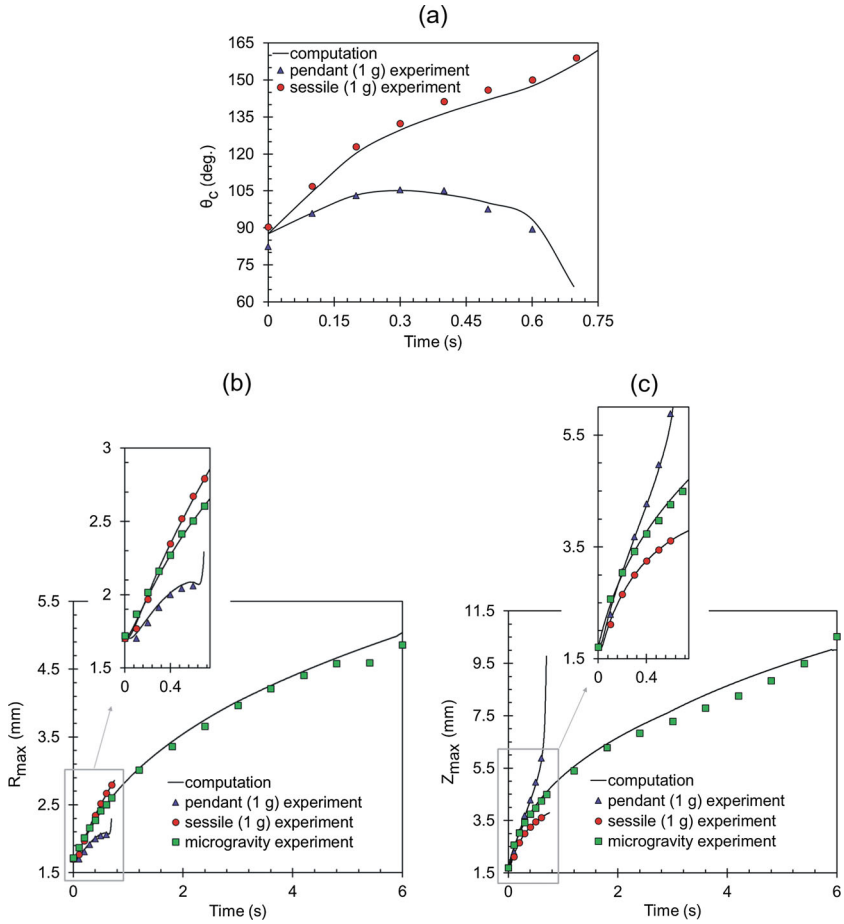

Fig. 7 **a** Plot showing comparison of computed and measured contact angles for the 1 g cases. **b** and **c** Plots showing comparison of computed and measured R_{max} and Z_{max} values for the 1 g and microgravity cases

Conclusions

Microgravity experiments were performed using a series of parabolic flights. These parabolic flight experiments demonstrated that 10 mm diameter water drops can be grown and pinned successfully between two sharp-edged glass tubes in 6 s of microgravity. Creating drops of this size within such a short time associated with each parabola, is encouraging for the prospects of drop formation and pinning aboard the ISS. FEM-based modeling using a commercial package was also performed for both ground-based (1 g) and microgravity cases. Comparison of computed and the measured droplet shapes showed a good match for the sessile drop (1 g) case. Agreement between computed and measured droplet shapes was also observed for the pendant drop (1 g) case prior to the pinch-off. Also, the computed and measured drop shapes agreed closely for the microgravity case prior to pinning of the drop to the needle-side ring. For later times, a departure was noticed between the computed and measured drop shapes due to an axial misalignment as well as a radial dislocation of the needle in the glass tube. However, once the drop was pinned at both rings and the drop growth stopped (at 6 s), the computed drop shape agreed well with the measured drop shape. Contact angle predicted by the computations was also compared with the measured values for the 1 g cases. It was found that the computed contact angle was in agreement with the measured contact angle. The computed and measured values of maximum radii, $R_{\max}$ and maximum height, $Z_{\max}$ of the drop were also compared. It was observed that the computed values of $R_{\max}$ agreed well with the measured values for all the cases. Also, the computed $Z_{\max}$ was in close agreement with the measured $Z_{\max}$ for the 1 g cases. For the microgravity case, the computed $Z_{\max}$ closely matched the measured $Z_{\max}$ prior to pinning of the drop to the needle-side ring, and beyond this time a fair agreement between the computed and measured $Z_{\max}$ values was observed. Overall, it was concluded that the computational models were able to predict the drop growth and pinning for both 1 g and microgravity cases. Future parabolic flight experiments that are planned to test growth and pinning of larger drops can benefit from these computational models which will help in designing such experiments. Also, these validated computational models will aid in designing the hardware for the implementation of RSD aboard the ISS. However, it must be noted that the use of these computational models is

limited to cases where the air-liquid interface is free from any surfactants or adsorbed protein. Additional modifications would be required to model the soluto-Marangoni effects as well as the effects of surface shear and dilatational viscosity for the cases where surfactants or proteins are present at the air-liquid interface.

Acknowledgments Many individuals have made significant contributions toward the results presented here. We thank Ellen Rabenberg (NASA-MSFC) for her efforts in preparing the parabolic flight hardware as well as performing some of the experiments. We are also grateful to Jeffery Quick (Jacobs Engineering and Science Services and Skill Augmentation, ESSSA group) for developing much of the parabolic flight hardware, including the pump control system. We thank Kevin Depew (NASA-MSFC) who assisted with facilitating the parabolic flight by doing structural and electrical analysis of the flight hardware. We thank Carole Fritsche (Stinger Ghaffarian Technologies, SGT) for her expertise in parabolic flight experiments both as a mentor and a performer herself. We acknowledge Assad A. Oberai (RPI) for his guidance on the computational modeling of droplet dynamics. We thank Sid Gorti (NASA-MSFC) who is the project scientist for his efforts and all the fruitful discussions over the years on many aspects of this project. We are grateful to Donnie Mccaghren (NASA-MSFC) who was the project manager for his tireless efforts and seeing this work to fruition. We thank Robert Roe (NASA-JSC) who was the project manager for the parabolic flight grant for his efforts to ensure a successful flight. Finally, we thank Juan M. Lopez (Arizona State University) for his involvement from the conception of this project to guiding the path toward the experiments aboard the ISS. This work was supported through NASA grants NNX13AQ22G and NNX15AJ83G.

References

Antar, B.N., Ethridge, E.C., Maxwell, D.: Viscosity measurement using drop coalescence in microgravity. Microgravity Sci. Technol. **14**, 9–19 (2003)

Bekard, I.B., Asimakis, P., Bertolini, J., Dunstan, D.E.: The effects of shear flow on protein structure and function. Biopolymers **95**, 733–745 (2011)

Bostwick, J.B., Steen, P.H.: Stability of constrained capillary surfaces. Annu. Rev. Fluid Mech. **47**, 539–568 (2015)

Brutin, D., Zhu, Z.Q., Rahli, O., Xie, J.C., Liu, Q.S., Tadrist, L.: Sessile drop in microgravity: creation, contact angle and interface. Microgravity Sci. Technol. **21**, 67–76 (2009)

Brutin, D., Zhu, Z.Q., Rahli, O., Xie, J.C., Liu, Q.S., Tadrist, L.: Evaporation of ethanol drops on a heated substrate under microgravity conditions. Microgravity Sci. Technol. **22**, 387–395 (2010)

Chen, A.U., Notz, P.K., Basaran, O.A.: Computational and experimental analysis of pinch-off and scaling. Phys. Rev. Lett. **88**, 174501–174504 (2002)

Chiang, R., Elliott, J.A.W.: A macroscopic solids-stabilized emulsion droplet model in reduced gravity. Microgravity Sci. Technol. **16**, 158–163 (2005)

Hayes, D.G.: Bioprocessing methods to prepare biobased surfactants for pharmaceutical products. American Pharmaceutical Rev., April 2011 http://www.americanpharmaceuticalreview.com/Featured-Articles/37032-Bioprocessing-Methods-to-Prepare-Biobased-Surfactants-for-Pharmaceutical-Products/ (2011)

Maa, Y.-F., Hsu, C.C.: Protein denaturation by combined effect of shear and air-liquid interface. Biotechnol. Bioeng. **54**, 503–512 (1997)

McBride, S.A., Tilger, C.F., Sanford, S.P., Tessier, P.M., Hirsa, A.H.: Comparison of human and bovine insulin amyloidogenesis under uniform shear. J. Phys. Chem. B **119**, 10426–10433 (2015)

Morinaga, A., Hasegawa, K., Nomura, R., Ookoshi, T., Ozawa, D., Goto, Y., Yamada, M., Naiki, H.: Critical role of interfaces and agitation on the nucleation of Aβ amyloid fibrils at low concentrations of Aβ monomers. B.B.A.-Proteins Proteom. **1804**, 986–995 (2010)

Nayagam, V., Haggard, J.B., Colantonio, R.O., Marchese, A.J., Dryer, F.L., Zhang, B.L., Williams, F.A.: Microgravity n-heptane droplet combustion in oxygen–helium mixtures at atmospheric pressure. AIAA J **36**, 1369–1378 (1998)

Nielsen, L., Khurana, R., Coats, A., Frokjaer, S., Brange, J., Vyas, S., Uversky, V.N., Fink, A.L.: Effect of environmental factors on the kinetics of insulin fibril formation: elucidation of the molecular mechanism. Biochemistry **40**, 6036–6046 (2001)

Posada, D.: Amyloid fibril formation in solution and at interfaces in shearing flows. Ph.D. thesis, Rensselaer Polytechnic Institute (2013)

Raghunandan, A., Lopez, J.M., Hirsa, A.H.: Bulk flow driven by a viscous monolayer. J. Fluid Mech. **785**, 283–300 (2015)

Savino, R., Nota, F., Fico, S.: Wetting and coalescence prevention of drops in a liquid matrix. Ground and parabolic flight results. Microgravity Sci. Technol. **14**, 3–12 (2003)

Sluzky, V., Tamada, J.A., Klibanov, A.M., Langer, R.: Kinetics of insulin aggregation in aqueous solutions upon agitation in the presence of hydrophobic surfaces. P. Natl. Acad. Sci. USA **88**, 9377–9381 (1991)

Stalder, A.F., Kulik, G., Sage, D., Barbieri, L., Hoffmann, P.: A snake-based approach to accurate determination of both contact points and contact angles. Colloid Surf. A **286**, 92–103 (2006)